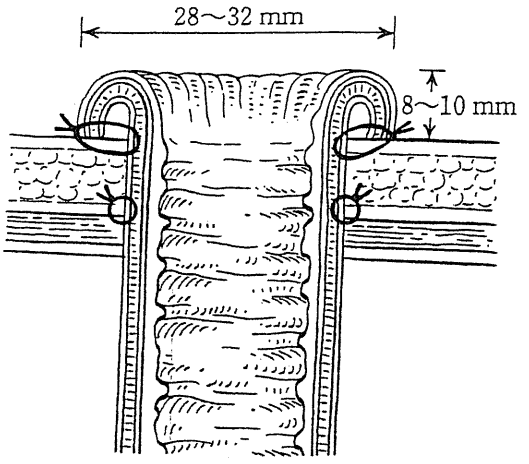

図 13　人工肛門造設
縁より便汁漏出防止のため平均的に直径 28±3 mm，高さ 10±2 mm とする。

し切除している尿管を Nesbit 法で吻合し，口側端を縫合閉鎖する。回腸導管の肛門側は回腸瘻となるが，皮膚まで持ち上げるため，ある程度の長さが必要である。縫合には結石防止のためすべて 4-0 吸収糸を使用している（図 12）。

人工肛門はヘルニア防止のために腹直筋内に造設するが（図 13），体型によってその位置が微妙に違ってくる。個々人が自然体で見える位置で，横皺のない平らで装具が貼りやすい所に造設している。手術終了時の腹会陰部を図 14，15 に示す。

ま と め

会陰皮膚を大きく切除したとき，1 期縫合するこ

図 14　薄筋による会陰部有茎移植完成図

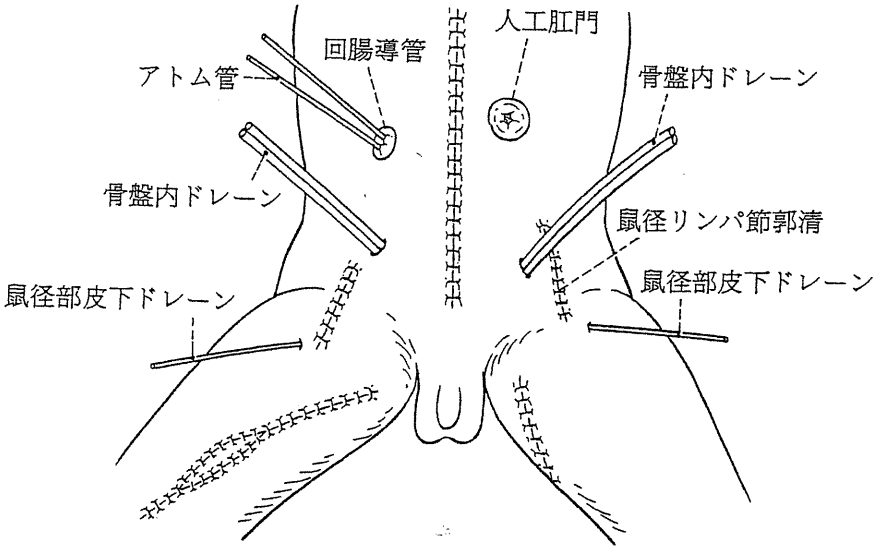

図 15　直腸肛門癌に対する骨盤内臓全摘ならびに薄筋による有茎筋皮弁移植完成図

とは，それが可能であっても，術後開脚障害を合併することは必至である。薄筋皮弁で有茎移植することは術後のQOLを高度に維持できる手技であると確信する。過去2年間で施行された6例の術後の経過を検討したが，支配血管周囲を十分に剝離していなく，回転が十分でなかった例に血行不良例があった。また，筋皮弁を採取した大腿部の筋力がやや低下している症例もあった。このことは今後の課題と考えられた。

文　献

1) 太田博俊ほか：腹会陰式直腸切断術．手術 49：1023—1031, 1995
2) 北条慶一：骨盤内臓摘除術．外科治療 51：13—25, 1984
3) Nesbit RM：Ureterosigmoid anastomosis by direct elliptical conection；A preliminary report. J Urol 61：728—734 1949

UICC
global cancer control

IJC
International Journal of Cancer

Synthetic siRNA targeting the breakpoint of *EWS/Fli-1* inhibits growth of Ewing sarcoma xenografts in a mouse model

Iori Takigami[1], Takatoshi Ohno[1], Yukio Kitade[2], Akira Hara[3], Akihito Nagano[1], Gou Kawai[1], Mitsuru Saitou[1], Aya Matsuhashi[1], Kazunari Yamada[1] and Katsuji Shimizu[1]

[1] Department of Orthopaedic Surgery, Gifu University Graduate School of Medicine, Gifu, Japan
[2] Department of Biomolecular Science, Faculty of Engineering, Gifu University, Gifu, Japan
[3] Department of Tumor Pathology, Gifu University Graduate School of Medicine, Gifu, Japan

The *EWS/Fli-1* fusion gene, a product of the translocation t(11;22, q24;q12), is detected in 85% of Ewing sarcomas and primitive neuroectodermal tumors. It is thought to be a transcriptional activator that plays a significant role in tumorigenesis. In this study, we developed a novel EWS/Fli-1 blockade system using RNA interference and tested its application for inhibiting the proliferation of Ewing sarcoma cells *in vitro* and the treatment of mouse tumor xenografts *in vivo*. We designed and synthesized a small interfering RNA (siRNA) possessing an aromatic compound at the 3′-end targeting the breakpoint of EWS/Fli-1. As this sequence is present only in tumor cells, it is a potentially relevant target. We found that the siRNA targeting EWS/Fli-1 significantly suppressed the expression of EWS/Fli-1 protein sequence specifically and also reduced the expression of c-Myc protein in Ewing sarcoma cells. We further demonstrated that inhibition of EWS/Fli-1 expression efficiently inhibited the proliferation of the transfected cells but did not induce apoptotic cell death. In addition, the siRNA possessing the aromatic compound at the 3′-end was more resistant to nucleolytic degradation than the unmodified siRNA. Administration of the siRNA with atelocollagen significantly inhibited the tumor growth of TC-135, a Ewing sarcoma cell line, which had been subcutaneously xenografted into mice. Moreover, modification of the 3′-end with an aromatic compound improved its efficiency *in vivo*. Our data suggest that specific downregulation of EWS/Fli-1 by RNA interference is a possible approach for the treatment of Ewing sarcoma.

The Ewing sarcoma family of tumors (ESFTs) is a group of highly malignant neoplasms that most often affect children and young adults in the first two decades of life. It is the second most common malignant bone tumor and accounts for approximately 10% of all primary bone tumors. Despite aggressive treatment strategies (chemotherapy, radiation therapy and surgery), the long-term disease-free survival rate of patients with ES is still disappointingly low, particularly in poor-risk patients with metastasis. Therefore, identification of new therapeutic targets is urgently needed.

The *EWS/Fli-1* fusion gene, a product of the translocation t(11;22, q24;q12), is detected in 85% of ESs and primitive neuroectodermal tumors. The EWS/Fli-1 translocation is formed by the *N*-terminal domain of the RNA-binding protein EWS and the DNA-binding domain of the ETS family transcriptional factor Fli-1. Identification of several breakpoints for both EWS and Fli-1 has demonstrated that the *EWS/Fli-1* fusion genes are heterogeneous. Breakpoints of Type 1 (Exon 7 of EWS/Exon 6 of Fli-1) and Type 2 (Exon 7 of EWS/Exon 5 of Fli-1) are most commonly detected in affected patients.[1–3] We have reported that the EWS/Fli-1 fusion protein may be a transcriptional activator that plays a significant role in the tumorigenesis of ESFTs.[4–7] Although substantial studies have reported that antagonism of the EWS fusion gene reduces tumorigenicity and clonogenicity,[8–10] its detailed biological targets remain unknown. Our previous studies have indicated that the *EWS/Fli-1* gene regulates telomerase reverse transcriptase (TERT),[11] phospholipase D2,[12] Aurora A, Aurora B[13] and vascular endothelial growth factor (VEGF).[14]

RNA interference (RNAi) is a process of sequence-specific posttranscriptional gene silencing triggered by double-stranded RNAs (dsRNAs). These dsRNAs are processed by the enzyme Dicer to generate duplexes of 21 to 23 nucleotides (nt). These duplexes, which contain a 2-nt overhang at the 3′-end of each strand, are termed short interfering RNAs

Key words: siRNA, sarcoma, xenograft, aromatic compound, atelocollagen

Abbreviations: ActD: actinomycin D; BrdU: 5-bromo-2′-deoxyuridine; dsRNAs: double-stranded RNAs; ESFTs: Ewing sarcoma family of tumors; FBS: fetal bovine serum; nt: nucleotides; ON: oligoribonucleotide; PI: propidium iodide; PARP: poly(ADP-ribose) polymerase; RISC: RNA-induced silencing complex; RNAi: RNA interference; siRNA: small interfering RNA; SVPD: snake venom phophodiesterase; TERT: telomerase reverse transcriptase; TUNEL: terminal deoxynucleotidyl transferase-mediated dUTP nick end labeling; VEGF: vascular endothelial growth factor

The authors declare that they have no competing interests.
DOI: 10.1002/ijc.25564
History: Received 4 Mar 2010; Accepted 8 Jul 2010; Online 20 Jul 2010

Correspondence to: Takatoshi Ohno, Department of Orthopaedic Surgery, Gifu University Graduate School of Medicine, 1-1 Yanagido, Gifu, 501-1194, Japan, Tel.: [+81-58-230-6333], Fax: +[81-58-230-6334], E-mail: takaohno@gifu-u.ac.jp

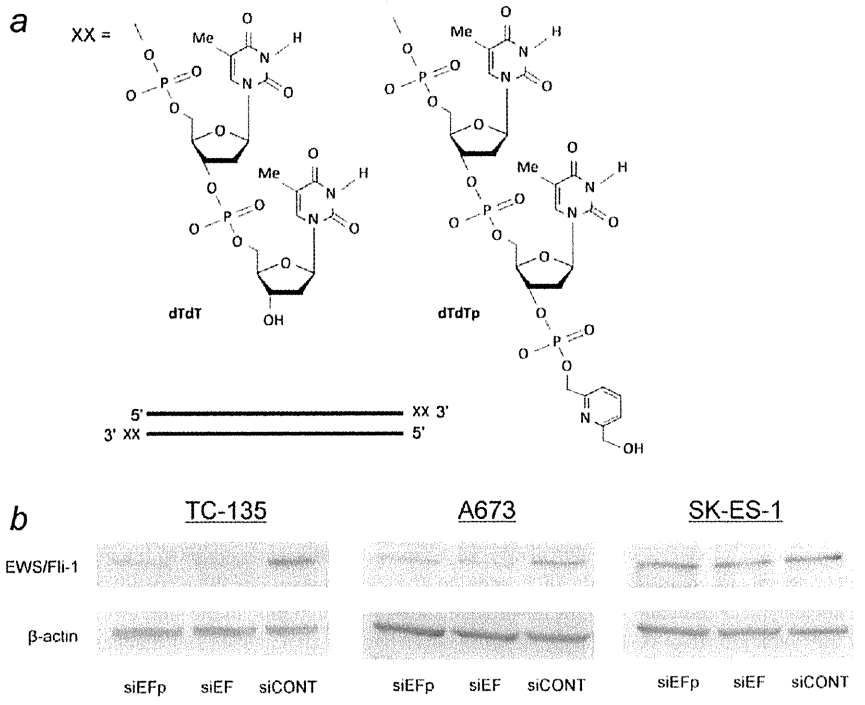

Figure 1. Characterization of the siRNAs. (*a*) Structures of the siRNAs. (*b*) Synthetic siRNAs targeting the breakpoint of EWS/Fli-1 Type 1 reduce the expression of EWS/Fli-1 protein in Ewing sarcoma cells. Western blot analysis of EWS/Fli-1 protein in TC-135, A673 and SK-ES-1 cells treated with siEFp, siEF, or siCONT at 48 hr after transfection. β-actin was used as a loading control. The results are representative of three independent experiments.

(siRNAs). These siRNAs associate with the RNA-induced silencing complex (RISC), which is then guided to catalyze the sequence-specific degradation of the target mRNA.[15,16] RNAi technologies offer the means to rationally design gene-specific inhibitors and are currently the most widely used techniques in functional genomic studies. However, application of siRNAs *in vivo* remains difficult because of problems associated with their stability, delivery and therapeutic efficacy.

Here, we demonstrate that silencing of EWS/Fli-1 with RNAi impairs both cell proliferation of ES cell lines and tumor growth in a mouse xenograft model. For our study, we used synthetic siRNA possessing an aromatic compound at the 3′-end and unmodified siRNA, targeting the breakpoint of the EWS/Fli-1 type 1 fusion transcript. Targeting of the EWS/Fli-1 chimeric oncogene using RNAi technology will set a paradigm for the validation of siRNA-based applications for treatment of ES, as EWS/Fli-1 is present only in tumor cells and absent in normal cells. Our results suggest that targeting of EWS/Fli-1 could be a possible therapeutic option for ES.

Material and Methods

The siRNAs

The siRNA was designed on the basis of the target sequence at the breakpoint of EWS/Fli-1 type 1. The unmodified siRNA (siEF) was synthesized by and purchased from Dharmacon (Lafayette, CO). The sense and antisense sequences were as follows: 5′-GCAGAACCCUUCUUAUGACdTdT-3′ (sense) and 5′-GUCAUAAGAAGGGUUCUGCdTdT-3′ (antisense). By using a DNA/RNA synthesizer by the phosphoramidite method, we designed and chemically synthesized siRNA possessing the aromatic compound pyridine (p) at the 3′-end (siEFp; Fig. 1*a*).[17,18] The sequences were 5′-GCAGAA CCCUUCUUAUGACdTdTp-3′ (sense) and 5′-GUCAUAAG AAGGGUUCUGCdTdTp-3′ (antisense). In addition, we synthesized siRNA with a 3′-end modification targeting *Renilla* luciferase (siCONT) as a negative control. The sequences were 5′-GGCCUUUCACUACUCCUCAdTdTp-3′ (sense) and 5′-GUACGAGUAGUGAAAGGCCdTdTp-3′ (antisense). A BLAST search against EST libraries was performed to confirm that no other human gene was targeted. All siRNAs were resuspended in RNase-free water to prepare a 20-μM stock solution.

Cell culture and transfection

TC-135, A673 and SK-ES-1 are ES cell lines carrying EWS/Fli-1. TC-135 and A673 have the EWS/Fli-1 Type 1 fusion, whereas SK-ES-1 has the Type 2 fusion. TC-135 was kindly supplied by Dr. T.J. Triche (University of Southern California, Los Angeles, CA). A673 and SK-ES-1 were purchased from the American Type Culture Collection (Manassas, VA).

TC-135 cells were maintained in RPMI 1640 medium (Invitrogen, Carlsbad, CA) containing 10% fetal bovine serum (FBS) at 37°C with a 5% CO_2 atmosphere. A673 cells were cultured in DMEM with 10% FBS at 37°C under a 10% CO_2 atmosphere. SK-ES-1 cells were cultured in McCoy's 5A medium with 10% FBS at 37°C under a 5% CO_2 atmosphere. Transfection was carried out in 60-mm dishes (at 40% confluency) using lipofectamine 2000 (Invitrogen), as recommended by the manufacturer. Total protein and mRNA were collected for Western blot analysis and real-time RT-PCR, respectively.

Western blot analysis

Western blot analysis was carried out exactly as described previously.[7,12] All proteins were determined by immunoblotting. The EWS/Fli-1 fusion protein (68 kDa) was sensitively detected by Western blotting using anti-Fli1 antibody (C-19, 1:200 dilution; Santa Cruz Biotechnology, Santa Cruz, CA). Mouse monoclonal antibodies against c-Myc (9E10, 1:200 dilution) and VEGF (C-1, 1:200 dilution) were obtained from Santa Cruz Biotechnology. Mouse monoclonal antibody against TERT (2C4, 1:1000 dilution) was obtained from Novus Biologicals (Littleton, CO). Rabbit polyclonal antibody against poly(ADP-ribose) polymerase (PARP) (9542, 1:1000 dilution) was obtained from Cell Signaling Technology (Boston, MA). Mouse monoclonal antibody against β-actin (JLA20, 1:5000 dilution) was obtained from Calbiochem (San Diego, CA). Quantitative changes in luminescence were estimated by LAS1000 UV mini and Multi Gauge Ver. 3.0 (Fuji Film, Tokyo, Japan).

Real-time quantitative RT-PCR

Total RNA was isolated using a RNeasy mini kit (*in vitro*) and a midi kit (*in vivo*; Qiagen, Hilden, Germany). Two micrograms of total RNA was reverse transcribed using a High-Capacity cDNA Reverse Transcription Kit with RNase inhibitor (Applied Biosystems, Foster City, CA). Quantitative real-time PCR analysis using the fluorescent SYBR green method (Bio-Rad, Richmond, CA) was performed in accordance with the manufacturer's instructions. The primers 5′-AGTTACCCACCCCAAACTGG-3′ (forward) and 5′-CCAAGGGGAGGACTTTTGTT-3′ (reverse) were used to amplify EWS/Fli-1, and the primers used for detection of GAPDH were 5′-TCCCATCACCATCTTCCA-3′ (forward) and 5′-ACTCACGCCACAGTTTCC-3′ (reverse). The PCR program consisted of enzyme activation at 95°C for 10 min followed by amplification for 40 cycles (95°C for 30 sec, 61°C for 30 sec, 72°C for 30 sec). Data were generated from each reaction, subjected to gene expression analysis using an iCycler iQ Real-Time PCR Detection System (Bio-Rad) and normalized against GAPDH.

Cell viability assay

Cell proliferation was determined by WST-8 assay using a Cell Counting Kit (Dojin, Kumamoto, Japan). Experiments were carried out in accordance with the manufacturer's recommended procedures. Briefly, cells (5×10^3 cells/well) were incubated overnight in a 96-well plate and then transfected with siRNA duplex. After incubation for the indicated time, the Cell Counting Kit reagents were added to the culture. After a further 1 hr of incubation, the absorbance at 450 nm was measured with a microplate reader. All experiments were performed at least four times.

Analysis of DNA synthesis by labeling with 5-bromo-2′-deoxyuridine

DNA synthesis was analyzed using a 5-bromo-2′-deoxyuridine (BrdU) Labeling and Detection Kit I (Roche Diagnostics, Mannheim, Germany). Experiments were carried out in accordance with the manufacturer's recommended procedures. Briefly, TC-135 cells grown on glass coverslips were treated with siRNAs (50 nM) as described above. After 72 hr of transfection, the cell culture medium was removed, and the BrdU-containing medium was added to the cells for 1 hr. The cells were then fixed with 70% ice-cold ethanol, and the BrdU was detected by immunofluorescence using anti-BrdU antibody. The cells were subsequently labeled with propidium iodide (PI) stain before being examined using a fluorescence microscope (BIOREVO BZ-9000; KEYENCE, Osaka, Japan).

Apoptosis detection

Apoptosis was assessed by terminal deoxynucleotidyl transferase-mediated dUTP nick end labeling (TUNEL) assay using an *In Situ* Cell Death Detection Kit (Roche). Experiments were carried out in accordance with the manufacturer's recommended procedures. Briefly, siRNA (50 nM)-treated TC-135 cells grown on glass coverslips were fixed with 4% paraformaldehyde in PBS, permeabilized with 0.2% Triton X-100 in PBS and stained with the TUNEL reaction mixture. The cells were finally labeled with Hoechst stain before being examined using a fluorescence microscope.

Serum stability

The siRNAs (5 μM) were incubated at 37°C in 10% FBS (Invitrogen) diluted in PBS. Aliquots of the reaction mixtures were collected at different times. The nuclease reactions were stopped by adding RNase inhibitor (Applied Biosystems). All samples were subjected to electrophoresis in 15% polyacrylamide-TBE under nondenaturing conditions and visualized by staining with GelRed (Biotium, Hayward, CA).

Partial hydrolysis of oligoribonucleotide with snake venom phosphodiesterase

Each oligoribonucleotide (ON) (300 pmol) labeled with fluorescein at the 5′-end was incubated with snake venom phosphodiesterase (SVPD) (5×10^{-3} units) in a buffer containing 37.5 mM Tris-HCl (pH 8.0) and 50 mM $MgCl_2$ (total 100 μL) at 37°C. At appropriate time points, aliquots of the reaction mixture were separated and added to a solution of 7 M urea. The solutions were analyzed by 20% polyacrylamide gel

containing 7 M urea. The labeled ON in the gel was visualized by a Bio-imaging analyzer (LAS-4000; Fuji Film).

Tumor therapy

Male BALB/c athymic (nu/nu) nude mice (7 weeks old) were obtained from Japan SLC (Tokyo, Japan). The mice were housed in the animal facilities of the Division of Animal Experiment, Life Science Research Center, Gifu University. A total of 3.0×10^6 TC-135 cells in 0.1 mL of serum-free RPMI1640 were inoculated subcuaneously through a 26-gauge needle into the posterior flank. Tumor diameters were measured with digital calipers, and the tumor volume in mm^3 was calculated using the formula: volume = $(\text{width})^2 \times \text{length}/2$. Once tumors had reached a volume of 50–60 mm^3 (Day 0), the tumor-bearing nude mice were treated with siEFp or siEF together with atelocollagen (Atelogene Local Use; Koken, Tokyo, Japan). The final concentration of atelocollagen was 1.75% and that of the siRNA was 500 pmol/tumor (10 μM in a 50-μL injection volume for each tumor). The dose of the siRNA was chosen on the basis of our previous study using VEGF siRNA mixed with atelocollagen against ES xenografts.[14] As a control, PBS mixed with atelocollagen was injected. Each therapeutic reagent was injected into the tumors on Days 0, 1, 3, 7, 14 and 21. Tumor growth was measured every 3 days for a period of up to 4 weeks. The mice were then sacrificed, and the tumors were removed at specified times during treatment or at the end of the experiment. Part of each tumor was snap frozen in liquid nitrogen for determination of EWS/Fli-1 mRNA levels by quantitative real-time RT-PCR, and another part was fixed in formalin for immunohistochemical analysis. Animal experiments in this study were performed in compliance with the guidelines of the Institute for Laboratory Animal Research, Gifu University Graduate School of Medicine, and the UCCCR guidelines for the Welfare of Animals in Experimental Neoplasia.

Immunohistochemistry

Tumor sections were dewaxed and rehydrated. Endogenous peroxidase activity was blocked with 3% H_2O_2 for 30 min. For Ki-67 staining, sections were blocked with 2% bovine serum albumin in PBS for 60 min and then incubated overnight at 4°C in a 1:100 dilution of anti-human Ki-67 monoclonal mouse antibody (Dako, Copenhagen, Denmark) in serum block. Subsequently, the sections were incubated with biotinylated secondary antibodies (LSAB2 kit; Dako) for 30 min, followed by incubation with peroxidase-labeled streptavidin (LSAB2 kit; Dako) for 30 min. The sections were developed with 3,3′-diaminobenzidine (DAB) and then counterstained with hematoxylin.

Statistical analysis

Statistical analyses were carried out using GraphPad Prism Version 5.01 (GraphPad Software, CA). The data were analyzed using ANOVA, and differences at $P < 0.05$ were considered statistically significant.

Results

Synthetic siRNAs targeting the breakpoint of EWS/Fli-1 type 1 reduce the expression of EWS/Fli-1 protein in TC-135 and A673 cells but not in SK-ES-1 cells

We designed two siRNAs targeting the breakpoint of EWS/Fli-1 Type 1: a siRNA possessing the aromatic compound pyridine in the 3′-overhang region (siEFp) and an unmodified siRNA (siEF). To investigate their sequence specificity, these siRNAs were used to treat TC-135 and A673 cells, which carry the Type 1 EWS/Fli-1 fusion, and SK-ES-1 cells, which carry the Type 2 fusion. Both siRNAs reduced the level of EWS/Fli-1 protein expression in TC-135 and A673 cells but had no apparent effect on that of SK-ES-1 cells (Fig. 1*b*). The siRNA targeting luciferase (siCONT) showed no effect.

Effects of synthetic siRNAs targeting the breakpoint of EWS/Fli-1 type 1 in TC-135 cells

The potency of the siRNA modified with the aromatic compound pyridine at the 3′-end was investigated by analyzing the levels of EWS/Fli-1 mRNA and protein in TC-135 cells at different time points after transfection. The siEFp (50 nM) and siEF (50 nM) significantly downregulated the expression of EWS/Fli-1 mRNA at 24 hr after transfection. However, at 72 hr after transfection, we found that the downregulation of EWS/Fli-1 mRNA by siEFp was significantly greater than that by siEF (Fig. 2*a*). Decreased mRNA levels were reflected at the protein levels. Figure 2*b* shows the results of immunoblot analysis and the relative intensities of EWS/Fli-1 protein expression standardized against β-actin. It was found that, at 48 hr after transfection, siEFp (50 nM) and siEF (50 nM) reduced the expression of EWS/Fli-1 protein to a similar extent. On the other hand, at 96 hr after transfection, siEFp downregulated the expression of EWS/Fli-1 protein to a greater degree than siEF. These inhibitory effects were dependent on the concentration of the siRNAs, and maximal suppression of EWS/Fli-1 protein was detected when 50 nM was used (Fig. 2*c*).

Because EWS/Fli-1 is known to activate the c-Myc promoter,[19] we tested whether siRNAs targeting EWS/Fli-1 had any effect on the level of c-Myc protein expression in TC-135 cells. It was found that the downregulation of EWS/Fli-1 protein caused by siEFp and siEF paralleled the downregulation of c-Myc protein (Fig. 2*d*). Our previous studies had shown that EWS/Fli-1 regulates TERT and VEGF.[11,14] Therefore, we checked whether EWS/Fli-1 inhibition affected the expression of these proteins. The results (Fig. 2*d*) showed that siEFp and siEF decreased the level of both TERT and VEGF.

EWS/Fli-1 knockdown correlates with decreased proliferation of ES cells

To study the cellular effects of EWS/Fli-1 knockdown in ES cell lines, TC-135, A673 and SK-ES-1 cells were transfected with the nonfunctional siCONT as a negative control or with

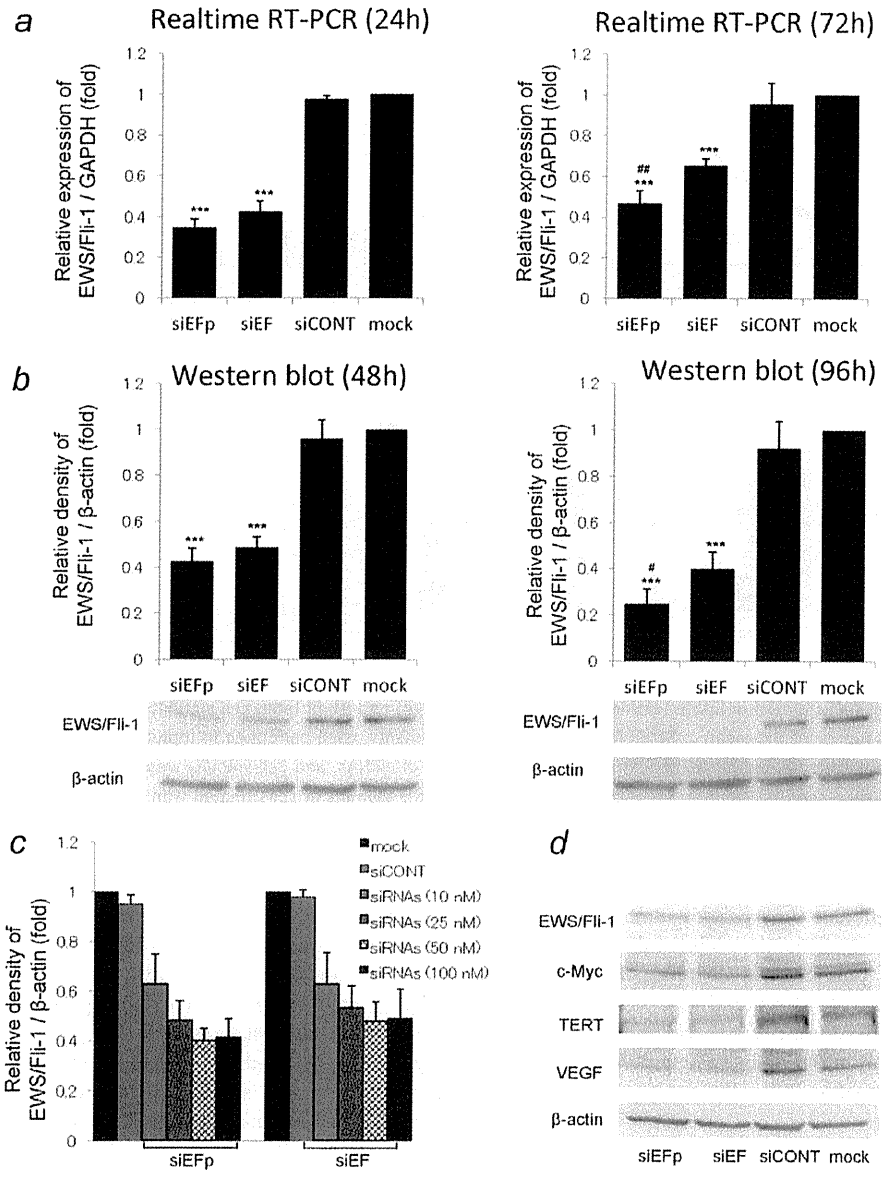

Figure 2. Effects of synthetic siRNAs targeting the breakpoint of EWS/Fli-1 Type 1 in TC-135 cells. TC-135 cells were transfected with siEFp, siEF, siCONT or lipofectamine alone (mock). (*a*) Decreased expression of EWS/Fli-1 mRNA at 24 hr (left) and 72 hr (right) after transfection with various siRNAs (50 nM). Knockdown efficiency was measured quantitatively by real-time reverse transcription-PCR (RT-PCR) analysis. Levels of EWS/Fli-1 mRNA expression were obtained subsequent to normalization with constitutively expressed GAPDH mRNA. Each bar represents the mean ± SD (n = 4 dishes). ***$P < 0.001$ *vs.* siCONT and mock. ##$P < 0.01$ *vs.* siEF. (*b*) Western blot analysis of EWS/Fli-1 protein performed on a lysate of TC-135 cells at 48 hr (left) and 96 hr (right) after transfection with siRNAs (50 nM). β-actin was used as a loading control. The bands of EWS/Fli-1 were quantified, and their ratios relative to β-actin were calculated. Each bar represents the mean ± SD (n = 4 dishes). ***$P < 0.001$ *vs.* siCONT and mock. #$P < 0.05$ *vs.* siEF. (*c*) Inhibition of EWS/Fli-1 protein expression in TC-135 cells transfected with the indicated amounts of siRNAs. The cells were harvested 48 hr after transfection, and cell extracts were analyzed by immunoblotting. β-actin was used as a loading control. Each bar represents the mean ± SD (n = 4 dishes). (*d*) siRNAs targeting EWS/Fli-1 (50 nM) downregulated the protein levels of c-Myc, TERT and VEGF, as shown by Western blot analysis. β-actin was used as a loading control. The results are representative of three independent experiments.

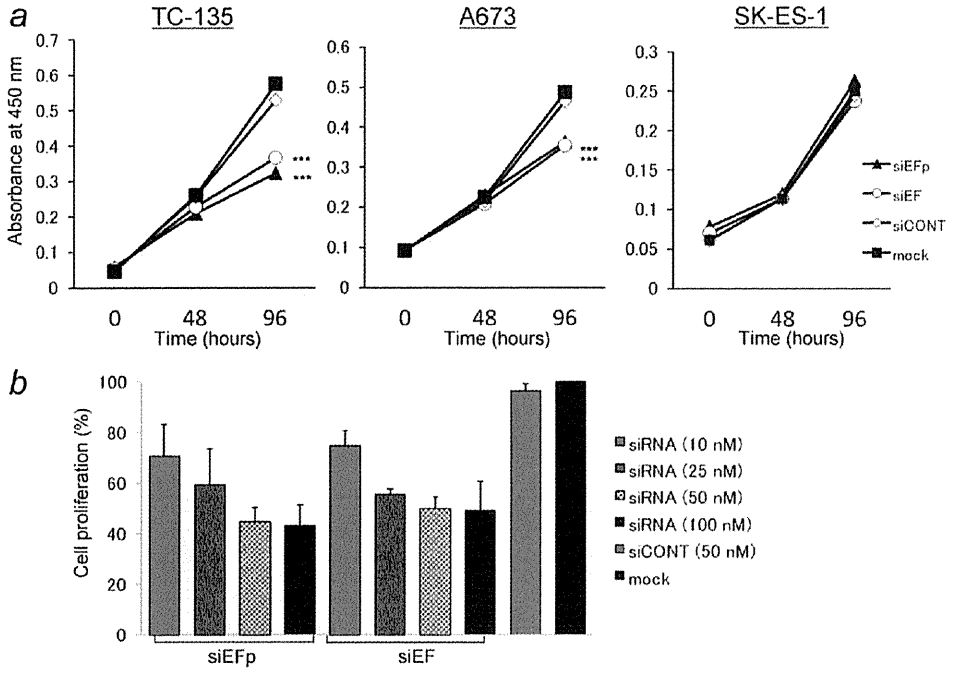

Figure 3. Effect of EWS/Fli-1 knockdown on proliferation of Ewing sarcoma cells. (*a*) TC-135, A673 and SK-ES-1 cells were treated with siEFp (50 nM), siEF (50 nM), siCONT (50 nM) or lipofectamine alone (mock). Forty-eight and 96 hr later, cell viability was determined with a Cell Counting Kit. The results represent the mean ± SD of four independent experiments, each performed in triplicate. ***$P < 0.001$ *vs.* siCONT and mock. (*b*) TC-135 cells were treated for 96 hr with the indicated amounts of siRNAs, and cell viability was determined with a Cell Counting Kit. The results represent the mean ± SD of cell viability relative to the viability of cells treated with mock.

the functional siEFp and siEF to specifically knockdown EWS/Fli-1. Cell proliferation was examined using a Cell Counting Kit over different time periods. Both siRNAs targeting EWS/Fli-1 Type 1 efficiently inhibited the proliferation of TC-135 and A673 cells but had no remarkable effect on SK-ES-1 cells (Fig. 3*a*). We also found that these growth-inhibitory effects were dependent on the concentration of the siRNAs (Fig. 3*b*). Thus, siEFp and siEF appear to exert antiproliferative activity against ES cells carrying the Type 1 *EWS/Fli-1* fusion gene.

Knockdown of EWS/Fli-1 by synthetic siRNAs in TC-135 cells impairs BrdU incorporation but does not induce apoptotic cell death

To investigate the mechanism of action of synthetic siRNAs targeting EWS/Fli-1, we used BrdU labeling to examine DNA synthesis during mitosis. In TC-135 cells treated for 72 hr with siEFp and siEF, we observed a significant decrease of BrdU-positive cells in comparison with siCONT- and mock-treated cells (Fig. 4*a*).

We then investigated whether the observed siRNA-induced reduction of viability occurred via induction of apoptosis, using TUNEL and Hoechst staining to measure nuclear condensation and fragmentation. TC-135 cells treated for 72 hr with siRNAs were stained with the *In Situ* Cell Death Detection Kit as described in "Materials and Methods." The results revealed no variations in the percentage of TUNEL-positive cells after any of the treatments (Fig. 4*b*).

An early transient burst of poly(ADP-ribosyl)ation of nuclear proteins has been shown to be required for apoptosis to proceed in various cell lines, followed by cleavage of PARP, catalyzed by caspase-3.[20,21] Although treatment of TC-135 cells with siEFp and siEF downregulated the expression of EWS/Fli-1, this did not result in accumulation of detectable levels of cleaved PARP (Fig. 4*c*). These results show that knockdown of the EWS/Fli-1 fusion protein by siEFp and siEF resulted in inhibition of cell proliferation, although apoptotic cell death was not induced.

Effect of 3′-end modification with an aromatic compound on siRNA stability

We examined the effect of nucleases on the stability of siRNA in FBS by modifying the 3′-end with an aromatic compound. As shown in Figure 5*a*, the unmodified siEF was fully degraded within 12 hr, whereas the modified siEFp showed only weak signs of degradation after 0.5, 1 and 3 hr. Increased stability was also observed with siEFp, where little full-length product remained at 12 hr.

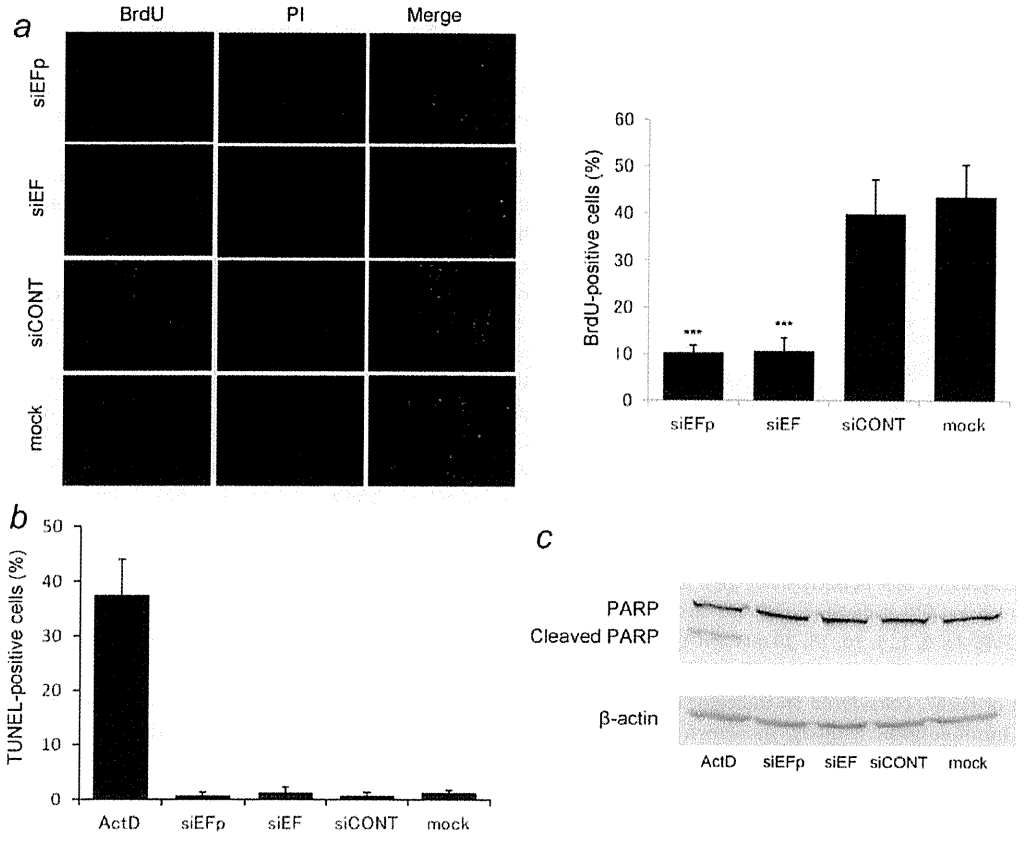

Figure 4. Knockdown of EWS/Fli-1 by synthetic siRNAs in TC-135 cells impairs BrdU incorporation but does not induce apoptotic cell death. (*a*) TC-135 cells were treated with siEFp, siEF, siCONT or lipofectamine alone (mock) for 72 hr. The results were representative immunofluorescent images after staining with BrdU (green) and PI (DNA, red). Quantitative data were obtained by counting BrdU-positive cells in five different fields per slide. The results represent the mean ± SD. ***$P < 0.001$ *vs.* siCONT and mock. (*b*) Similarly treated TC-135 cells were stained using an In Situ Cell Death Detection Kit, followed by Hoechst labeling. The number of TUNEL-positive cells was counted and the ratio calculated in five different fields per slide. As positive controls, cells incubated for 6 hr with 50 ng/mL actinomycin D (ActD) were analyzed. (*c*) TC-135 cells were treated with siRNAs for 96 hr and lysed, and protein samples were then separated by SDS-PAGE. The intact (116 kDa) and catalyzed (89 kDa) forms of PARP protein were detected by using anti-PARP antibody. As positive controls, protein samples from the cells treated with 50 ng/mL ActD for 6 hr were analyzed. β-actin was used as a loading control. The results are representative of three independent experiments.

Next, the susceptibility of the ON to SVPD, a 3′-exonuclease, was examined. The antisense strands of siEF and siEFp labeled at the 5′-end with fluorescein were incubated with SVPD. The reactions were analyzed with PAGE. Figure 5*b* shows the results. The unmodified siEF was hydrolyzed randomly after 5 min of incubation, whereas the modified siEFp was resistant to enzyme. Taken together, our data demonstrate that 3′-end modification with an aromatic compound on siRNA can increase nuclease resistance.

Treatment of TC-135 xenografts with siRNAs targeting EWS/Fli-1

We next investigated the therapeutic effectiveness of siRNAs targeting EWS/Fli-1. We established a xenograft model of TC-135 cells as described in "Materials and Methods" and examined intratumoral treatment with siRNAs targeting EWS/Fli-1 together with atelocollagen. When the tumors reached a volume of 50–60 mm^3, the animals were randomized into four groups—siEFp, siEF, siCONT and PBS—and tumor growth was followed up over a period of up to 4 weeks. As shown in Figure 6*a*, siEFp and siEF markedly suppressed tumor growth in comparison with siCONT or PBS. Moreover, we found that siEFp significantly inhibited tumor growth in comparison with siEF. No death, loss of body weight or gross adverse effects occurred in the mice as a result of treatment with the siRNAs. Furthermore, application of siRNAs targeting EWS/Fli-1 decreased the production of EWS/Fli-1 mRNA in the tumors (Fig. 6*b*). We also examined

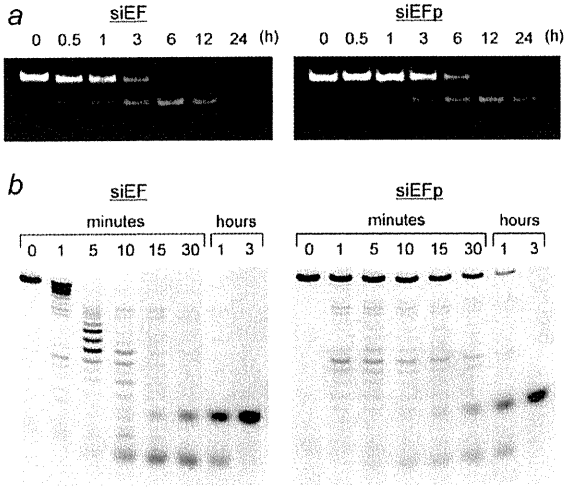

Figure 5. Analysis of siRNA stability. (*a*) siEF and siEFp were incubated in 10% FBS at 37°C for 0, 0.5, 1, 3, 6, 12 or 24 hr, and aliquots were analyzed on 15% polyacrylamide gels. (*b*) 20% PAGE of 5′-fluorescein-labeled ONs hydrolyzed by SVPD. ONs were incubated with SVPD for 0, 1, 5, 10, 15, 30 min and 1 and 3 hr.

the expression of Ki-67, considered an indicator of cell proliferation, using immunohistochemistry. As shown in Figure 6*c*, the percentage of Ki-67-positive cells was significantly reduced in tumors from mice treated with siEFp and siEF.

Discussion

ESFTs are very aggressive pediatric malignancies. Despite the use of multimodal therapy, their prognosis remains poor, with an overall 5-yr survival of 55–65% in patients with localized disease, or even lower in poor-risk patients.[22,23] These tumors are characterized by the presence, in over 85% of cases, of a chromosomal translocation that results in the generation of the chimeric gene, *EWS/Fli-1*. We have already studied EWS/Fli-1 and established some of the effects of this oncoprotein.[4–10,12–14] The results obtained so far indicate that EWS/Fli-1 has potential as a unique therapeutic target for the treatment of ESFTs. Inhibition of the expression of EWS/Fli-1 in ES cells using antisense oligonucleotide results in decreased proliferation, suggesting a potential therapeutic intervention directed at this oncogene.[24–26] Reduction of EWS/Fli-1 by siRNA has recently been investigated by other groups.[27–29] However, to our knowledge, no previous report has indicated that chemically synthesized siRNA targeting the breakpoint of EWS/Fli-1 with non-viral delivery inhibits the growth of human ES subcutaneous xenografts. This study demonstrated that knockdown of EWS/Fli-1 using synthetic siRNAs inhibited both the proliferation of ES cells and the growth of human ES tumor xenografts in a mouse model.

The silencing of gene expression by siRNA is a powerful tool for genetic analysis of mammalian cells and has the potential for further development into a specific, potent and safe treatment for human disease. However, application of siRNAs *in vivo* and their possible use for therapy still has several critical hurdles that have not yet been comprehensively addressed. For instance, the delivery, stability and pharmacokinetics of siRNA are major problems. So far, many types of siRNAs modified at the base or carrying sugar or phosphate moieties have been synthesized, and their nuclease-resistant properties and RNAi-inducing activities have been studied.[30–33] Recently, we have developed and synthesized siRNAs possessing aromatic compounds at the 3′-end.[17,18] In this study, we first confirmed that siEFp significantly downregulated the expression of EWS/Fli-1 mRNA and protein and decreased the proliferation of ES cells. We then demonstrated that siEFp significantly inhibited tumor growth in our xenograft model. Furthermore, it was of considerable interest that siEFp was more potent than siEF against tumor xenografts *in vivo* despite the lack of significant changes observed in the *in vitro* proliferation. To test whether these modifications were capable of increasing the stability of siRNA, we incubated siEFp and siEF in bovine serum or SVPD, followed by separation on polyacrylamide gels. It was found that 3′-end modification with the aromatic compound was effective for improving the nuclease resistance of the siRNAs. These characteristics potentially improved the efficacy of siEFp, especially *in vivo*, where sustained delivery will be one major obstacle. In addition, to overcome the problem related to siRNA delivery, we used atelocollagen as a carrier of siRNAs in an *in vivo* experiment, as described previously.[14,34–38] It is known that atelocollagen has the ability to extend the half-life of siRNA and to keep it intact when embedded in the body. Atelocollagen is already used clinically and considered to be innocuous. Therefore, we consider that the clinical application of chemically synthesized siRNA with atelocollagen represents a simple and an attractive delivery system for siRNA *in vivo*.

Argonaute2, a key component of RISC, is responsible for mRNA cleavage in the RNAi pathway.[39,40] It is composed of PAZ, Mid and PIWI domains. X-ray structural analysis and nuclear magnetic resonance studies have revealed that the 3′-overhanging region of the guide strand (antisense strand) of siRNA is recognized by the PAZ domain and is accommodated into its hydrophobic binding pocket.[41–43] We hypothesized that the introduction of a lipophilic aromatic compound at the 3′-end of the siRNA would improve the affinity of the 3′-end for the PAZ domain, thus improving the effectiveness of the siRNA in comparison with the unmodified form.

The *c-Myc*, a proto-oncogene, is expressed at high levels in most human cancers and encodes a transcription factor implicated in various cellular processes such as cell growth, proliferation and loss of differentiation.[44] Downregulation of *c-Myc* could, therefore, play a role in a potential therapeutic strategy against human cancers.[45,46] Previous studies have indicated that c-Myc transcription is strongly upregulated by EWS/Fli-1.[19,47] In this study, we found that EWS/Fli-1

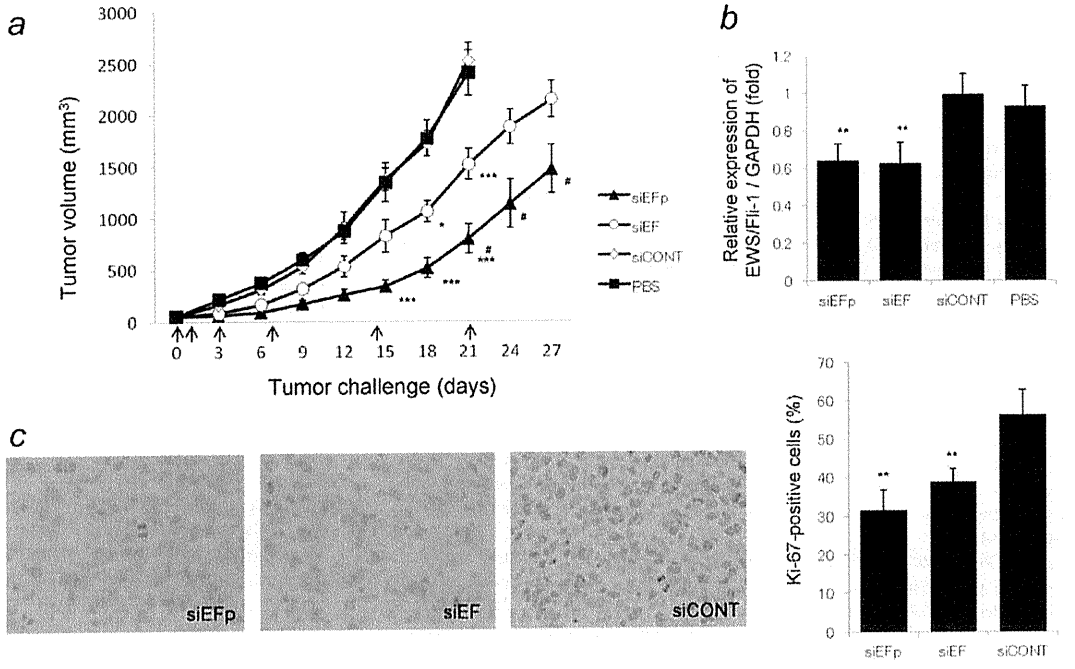

Figure 6. Inhibition of tumor growth by synthetic siRNAs targeting EWS/Fli-1 in the TC-135 xenograft model. (*a*) Tumor growth curves after treatment with siEFp, siEF, siCONT or PBS. Each therapeutic reagent was injected into the tumors on days 0, 1, 3, 7, 14 and 21 (arrows). The results represent mean ± SE (n = 6 tumors). $^{*}P < 0.05$; $^{***}P < 0.001$, when compared with siCONT and PBS. $^{\#}P < 0.05$ when compared with siEF. (*b*) Levels of EWS/Fli-1 mRNA in tumors were quantified by real-time quantitative RT-PCR. Each bar represents the mean ± SD (n = 4 tumors). $^{**}P < 0.01$ *vs.* siCONT and PBS. (*c*) Representative micrographs of immunohistochemical detection of Ki-67 in tumors induced by injection into nude mice of TC-135 cells treated as indicated (left). Ki-67-positive cells were counted in each of five independent areas. The percentage of Ki-67-positive cells was then calculated. The results represent the mean ± SD. $^{**}P < 0.01$ versus siCONT. Data are those for tumors excised 3 days into the treatment schedule.

knockdown by siRNA resulted in downregulation of c-Myc protein expression (Figure 2*c*). These results indicate that administration of siRNAs targeting EWS/Fli-1 may induce suppression of ES cell growth through the downregulation of c-Myc.

The tumor growth-inhibitory effect of synthetic siRNAs resulted from specific silencing of EWS/Fli-1. A decrease of EWS/Fli-1 mRNA expression was indeed observed by real-time quantitative RT-PCR of RNA extracted from siRNA-treated tumors. In this study, we also demonstrated that sequence-specific downregulation of EWS/Fli-1 impaired cell proliferation but did not induce apoptosis. It is noteworthy that the chemically synthesized siRNAs used in this study targeted the breakpoint of EWS/Fli-1 Type 1, and we found that these siRNAs reduced both the expression of EWS/Fli-1 protein and the proliferation of ES cells carrying EWS/Fli-1 Type 1 but not cells carrying Type 2. Moreover, our data showed that suppression of EWS/Fli-1 expression resulted in downregulation of the EWS/Fli-1-downstream targets, c-Myc, TERT and VEGF. Although off-target effects of siRNA cannot be completely ruled out, our current results indicate that EWS/Fli-1 inhibition is an attractive strategy for the treatment of ES, as this target sequence is present only in tumor cells.

In summary, we have shown that synthetic siRNAs targeting EWS/Fli-1 downregulate the expression of EWS/Fli-1 protein sequence specifically and also reduce the expression of c-Myc protein. We have also shown that inhibition of EWS/Fli-1 expression efficiently inhibits the proliferation and tumor growth of ES cells. Moreover, we have demonstrated that modification of siRNA with the aromatic compound pyridine at the 3′-end enhances the efficacy of treatment *in vivo*. These results suggest that specific downregulation of EWS/Fli-1 by synthetic siRNA is a possible approach for the treatment of ES. Simultaneous use of chemotherapy might also be effective. Further preclinical studies are warranted to explore the applicability of EWS/Fli-1 targeting for therapy of ES.

Acknowledgements

The authors thank Dr. T.J. Triche (University of Southern California, Los Angeles, CA) for providing the Ewing sarcoma cells and Takatoshi Yamamoto, Ayako Taguchi and Remi Nakashima for useful discussion and assistance.

References

1. Delattre O, Zucman J, Plougastel B, Desmaze C, Melot T, Peter M, Kovar H, Joubert I, de Jong P, Rouleau G, et al. Gene fusion with an ETS DNA-binding domain caused by chromosome translocation in human tumours. *Nature* 1992;359:162–5.
2. May WA, Gishizky ML, Lessnick SL, Lunsford LB, Lewis BC, Delattre O, Zucman J, Thomas G, Denny CT. Ewing sarcoma 11;22 translocation produces a chimeric transcription factor that requires the DNA-binding domain encoded by FLI1 for transformation. *Proc Natl Acad Sci U S A* 1993;90:5752–6.
3. Zucman J, Melot T, Desmaze C, Ghysdael J, Plougastel B, Peter M, Zucker JM, Triche TJ, Sheer D, Turc-Carel C, et al. Combinatorial generation of variable fusion proteins in the Ewing family of tumours. *EMBO J* 1993;12:4481–7.
4. Ohno T, Rao VN, Reddy ES. EWS/Fli-1 chimeric protein is a transcriptional activator. *Cancer Res* 1993;53: 5859–63.
5. Ohno T, Ouchida M, Lee L, Gatalica Z, Rao VN, Reddy ES. The EWS gene, involved in Ewing family of tumors, malignant melanoma of soft parts and desmoplastic small round cell tumors, codes for an RNA binding protein with novel regulatory domains. *Oncogene* 1994; 9:3087–97.
6. Rao VN, Ohno T, Prasad DD, Bhattacharya G, Reddy ES. Analysis of the DNA-binding and transcriptional activation functions of human Fli-1 protein. *Oncogene* 1993;8:2167–73.
7. Yamamoto T, Ohno T, Wakahara K, Nagano A, Kawai G, Saitou M, Takigami I, Matsuhashi A, Yamada K, Shimizu K. Simultaneous inhibition of mitogen-activated protein kinase and phosphatidylinositol 3-kinase pathways augment the sensitivity to actinomycin D in Ewing sarcoma. *J Cancer Res Clin Oncol* 2009;135:1125–36.
8. Ouchida M, Ohno T, Fujimura Y, Rao VN, Reddy ES. Loss of tumorigenicity of Ewing's sarcoma cells expressing antisense RNA to EWS-fusion transcripts. *Oncogene* 1995;11:1049–54.
9. Dohjima T, Ohno T, Banno Y, Nozawa Y, Wen-yi Y, Shimizu K. Preferential down-regulation of phospholipase C-beta in Ewing's sarcoma cells transfected with antisense EWS-Fli-1. *Br J Cancer* 2000;82: 16–9.
10. Dohjima T, Lee NS, Li H, Ohno T, Rossi JJ. Small interfering RNAs expressed from a Pol III promoter suppress the EWS/Fli-1 transcript in an Ewing sarcoma cell line. *Mol Ther* 2003;7:811–6.
11. Takahashi A, Higashino F, Aoyagi M, Yoshida K, Itoh M, Kyo S, Ohno T, Taira T, Ariga H, Nakajima K, Hatta M, Kobayashi M, et al. EWS/ETS fusions activate telomerase in Ewing's tumors. *Cancer Res* 2003;63:8338–44.
12. Nozawa S, Ohno T, Banno Y, Dohjima T, Wakahara K, Fan DG, Shimizu K. Inhibition of platelet-derived growth factor-induced cell growth signaling by a short interfering RNA for EWS-Fli1 via down-regulation of phospholipase D2 in Ewing sarcoma cells. *J Biol Chem* 2005;280: 27544–51.
13. Wakahara K, Ohno T, Kimura M, Masuda T, Nozawa S, Dohjima T, Yamamoto T, Nagano A, Kawai G, Matsuhashi A, Saitoh M, Takigami I, et al. EWS-Fli1 up-regulates expression of the Aurora A and Aurora B kinases. *Mol Cancer Res* 2008;6: 1937–45.
14. Nagano A, Ohno T, Shimizu K, Hara A, Yamamoto T, Kawai G, Saitou M, Takigami I, Matsuhashi A, Yamada K, Takei Y. EWS/Fli-1 chimeric fusion gene upregulates vascular endothelial growth factor-A. *Int J Cancer* 2010;126:2790–8.
15. Elbashir SM, Lendeckel W, Tuschl T. RNA interference is mediated by 21- and 22-nucleotide RNAs. *Genes Dev* 2001;15: 188–200.
16. Elbashir SM, Harborth J, Lendeckel W, Yalcin A, Weber K, Tuschl T. Duplexes of 21-nucleotide RNAs mediate RNA interference in cultured mammalian cells. *Nature* 2001;411:494–8.
17. Ueno Y, Inoue T, Yoshida M, Yoshikawa K, Shibata A, Kitamura Y, Kitade Y. Synthesis of nuclease-resistant siRNAs possessing benzene-phosphate backbones in their 3′-overhang regions. *Bioorg Med Chem Lett* 2008;18:5194–6.
18. Ueno Y, Watanabe Y, Shibata A, Yoshikawa K, Takano T, Kohara M, Kitade Y. Synthesis of nuclease-resistant siRNAs possessing universal overhangs. *Bioorg Med Chem* 2009;17:1974–81.
19. Bailly RA, Bosselut R, Zucman J, Cormier F, Delattre O, Roussel M, Thomas G, Ghysdael J. DNA-binding and transcriptional activation properties of the EWS-FLI-1 fusion protein resulting from the t(11;22) translocation in Ewing sarcoma. *Mol Cell Biol* 1994;14:3230–41.
20. Boulares AH, Yakovlev AG, Ivanova V, Stoica BA, Wang G, Iyer S, Smulson M. Role of poly(ADP-ribose) polymerase (PARP) cleavage in apoptosis. Caspase 3-resistant PARP mutant increases rates of apoptosis in transfected cells. *J Biol Chem* 1999;274:22932–40.
21. Simbulan-Rosenthal CM, Rosenthal DS, Iyer S, Boulares AH, Smulson ME. Transient poly(ADP-ribosyl)ation of nuclear proteins and role of poly(ADP-ribose) polymerase in the early stages of apoptosis. *J Biol Chem* 1998;273:13703–12.
22. Kontny U. Regulation of apoptosis and proliferation in Ewing's sarcoma—opportunities for targeted therapy. *Hematol Oncol* 2006;24:14–21.
23. Rodriguez-Galindo C, Spunt SL, Pappo AS. Treatment of Ewing sarcoma family of tumors: current status and outlook for the future. *Med Pediatr Oncol* 2003;40: 276–87.
24. Matsumoto Y, Tanaka K, Nakatani F, Matsunobu T, Matsuda S, Iwamoto Y. Downregulation and forced expression of EWS-Fli1 fusion gene results in changes in the expression of G(1)regulatory genes. *Br J Cancer* 2001;84:768–75.
25. Mateo-Lozano S, Gokhale PC, Soldatenkov VA, Dritschilo A, Tirado OM, Notario V. Combined transcriptional and translational targeting of EWS/FLI-1 in Ewing's sarcoma. *Clin Cancer Res* 2006;12:6781–90.
26. Lambert G, Bertrand JR, Fattal E, Subra F, Pinto-Alphandary H, Malvy C, Auclair C, Couvreur P. EWS fli-1 antisense nanocapsules inhibits ewing sarcoma-related tumor in mice. *Biochem Biophys Res Commun* 2000;279:401–6.
27. Toub N, Bertrand JR, Tamaddon A, Elhamess H, Hillaireau H, Maksimenko A, Maccario J, Malvy C, Fattal E, Couvreur P. Efficacy of siRNA nanocapsules targeted against the EWS-Fli1 oncogene in Ewing sarcoma. *Pharm Res* 2006;23:892–900.
28. Matsunobu T, Tanaka K, Nakamura T, Nakatani F, Sakimura R, Hanada M, Li X, Okada T, Oda Y, Tsuneyoshi M, Iwamoto Y. The possible role of EWS-Fli1 in evasion of senescence in Ewing family tumors. *Cancer Res* 2006;66:803–11.
29. Chansky HA, Barahmand-Pour F, Mei Q, Kahn-Farooqi W, Zielinska-Kwiatkowska A, Blackburn M, Chansky K, Conrad EU, 3rd, Bruckner JD, Greenlee TK, Yang L. Targeting of EWS/FLI-1 by RNA interference attenuates the tumor phenotype of Ewing's sarcoma cells in vitro. *J Orthop Res* 2004;22:910–7.
30. Braasch DA, Jensen S, Liu Y, Kaur K, Arar K, White MA, Corey DR. RNA interference in mammalian cells by chemically-modified RNA. *Biochemistry* 2003;42:7967–75.
31. Czauderna F, Fechtner M, Dames S, Aygun H, Klippel A, Pronk GJ, Giese K, Kaufmann J. Structural variations and stabilising modifications of synthetic siRNAs in mammalian cells. *Nucleic Acids Res* 2003;31:2705–16.
32. Amarzguioui M, Holen T, Babaie E, Prydz H. Tolerance for mutations and chemical

modifications in a siRNA. *Nucleic Acids Res* 2003;31:589–95.
33. Elmen J, Thonberg H, Ljungberg K, Frieden M, Westergaard M, Xu Y, Wahren B, Liang Z, Orum H, Koch T, Wahlestedt C. Locked nucleic acid (LNA) mediated improvements in siRNA stability and functionality. *Nucleic Acids Res* 2005;33: 439–47.
34. Minakuchi Y, Takeshita F, Kosaka N, Sasaki H, Yamamoto Y, Kouno M, Honma K, Nagahara S, Hanai K, Sano A, Kato T, Terada M, et al. Atelocollagen-mediated synthetic small interfering RNA delivery for effective gene silencing in vitro and in vivo. *Nucleic Acids Res* 2004;32:e109.
35. Takei Y, Kadomatsu K, Yuzawa Y, Matsuo S, Muramatsu T. A small interfering RNA targeting vascular endothelial growth factor as cancer therapeutics. *Cancer Res* 2004;64: 3365–70.
36. Takei Y, Kadomatsu K, Goto T, Muramatsu T. Combinational antitumor effect of siRNA against midkine and paclitaxel on growth of human prostate cancer xenografts. *Cancer* 2006;107:864–73.
37. Ochiya T, Nagahara S, Sano A, Itoh H, Terada M. Biomaterials for gene delivery: atelocollagen-mediated controlled release of molecular medicines. *Curr Gene Ther* 2001; 1:31–52.
38. Ochiya T, Takahama Y, Nagahara S, Sumita Y, Hisada A, Itoh H, Nagai Y, Terada M. New delivery system for plasmid DNA in vivo using atelocollagen as a carrier material: the Minipellet. *Nat Med* 1999;5:707–10.
39. Hammond SM, Boettcher S, Caudy AA, Kobayashi R, Hannon GJ. Argonaute2, a link between genetic and biochemical analyses of RNAi. *Science* 2001;293: 1146–50.
40. Martinez J, Patkaniowska A, Urlaub H, Luhrmann R, Tuschl T. Single-stranded antisense siRNAs guide target RNA cleavage in RNAi. *Cell* 2002;110:563–74.
41. Lingel A, Simon B, Izaurralde E, Sattler M. Structure and nucleic-acid binding of the *Drosophila argonaute* 2 PAZ domain. *Nature* 2003;426:465–9.
42. Yan KS, Yan S, Farooq A, Han A, Zeng L, Zhou MM. Structure and conserved RNA binding of the PAZ domain. *Nature* 2003; 426:468–74.
43. Ma JB, Ye K, Patel DJ. Structural basis for overhang-specific small interfering RNA recognition by the PAZ domain. *Nature* 2004;429:318–22.
44. Pelengaris S, Khan M, Evan G. c-MYC: more than just a matter of life and death. *Nat Rev Cancer* 2002;2:764–76.
45. Wang YH, Liu S, Zhang G, Zhou CQ, Zhu HX, Zhou XB, Quan LP, Bai JF, Xu NZ. Knockdown of c-Myc expression by RNAi inhibits MCF-7 breast tumor cells growth in vitro and in vivo. *Breast Cancer Res* 2005;7:R220–8.
46. Zhang X, Ge YL, Tian RH. The knockdown of c-myc expression by RNAi inhibits cell proliferation in human colon cancer HT-29 cells in vitro and in vivo. *Cell Mol Biol Lett* 2009;14:305–18.
47. Dauphinot L, De Oliveira C, Melot T, Sevenet N, Thomas V, Weissman BE, Delattre O. Analysis of the expression of cell cycle regulators in Ewing cell lines: EWS-FLI-1 modulates p57KIP2and c-Myc expression. *Oncogene* 2001;20:3258–65.

Tohoku J. Exp. Med., 2011, **223**, 75-78

Lipoblastoma Mimicking Myxoid Liposarcoma: A Clinical Report and Literature Review

Akihito Nagano,[1] Takatoshi Ohno,[1] Yutaka Nishimoto,[1] Yoshinobu Hirose,[2] Satoru Miyake[1] and Katsuji Shimizu[1]

[1]Department of Orthopedic Surgery, Graduate school of Medicine, Gifu University, Gifu, Japan
[2]Department of Tumor Pathology, Graduate School of Medicine, Gifu University, Gifu, Japan

Lipoblastoma is an uncommon benign lipomatous tumor, occurring typically in children less than 3 years of age. The magnetic resonance image (MRI) is a useful tool for diagnosis of lipoblastoma; its imaging typically shows high-intensity signals on both T1-weighted (T1-W) and T2 weighted (T2-W) images. Here, we present a 12-year-old female patient with a painless mass on the anterior right shoulder. MRI showed the mass with low-intensity signals on T1-W and high-intensity signals on T2-W images. Because of the atypical age and MRI findings, it was difficult to make a conclusive diagnosis of the tumor as lipoblastoma preoperatively. Histopathological examination of the excised tumor showed spindle-shaped or stellate cells embedded in the myxoid matrix, and a few small irregular clusters of mature fat cells that are separated by connective tissue septa. There were some immature, lipoblast-like cells dispersed. These findings are consistent with lipoblastoma, and myxoid liposarcoma was considered as one of the differential diagnosis. We finally diagnosed the tumor as a lipoblastoma for the reasons that there were many mature fat cells and no atypical cells for a myxoid liposarcoma. The postoperative course was uneventful and no recurrence was observed 5 years after the operation. The patient presented is worthy of note due to the unusual characteristics of the tumor. Even in the case of adolescent or older patients with atypical imaging, lipoblastoma should be considered as one of differential diagnosis.

Keywords: lipoblastoma; neoplasm; magnetic resonance imaging; adipose tumor; soft tissue tumor
Tohoku J. Exp. Med., 2011, **223** (1), 75-78.

Lipoblastoma is a rare benign soft-tissue childhood tumor occurring most commonly in children less than 3 years of age (Chung and Enzinger 1973; Mentzel et al. 1993), and magnetic resonance image (MRI) is a useful tool for its diagnosis and preoperative evaluation (Reiseter et al. 1999). MRIs of this type of tumor are typically characterized by high-intensity signals on both T1 weighted (T1-W) and T2 weighted (T2-W) images (Letourneau et al. 1993). We report a 12-year-old female patient with lipoblastoma in the shoulder, which was difficult to diagnose preoperatively because of the age and its atypical MRI findings. Meanwhile, the presented tumor showed generally low-intensity signals on T1-W, and high-intensity signals on T2-W images. These findings were not consistent with lipomatous tumor, and finally we made a diagnosis considering all findings obtained.

Clinical Findings

A 12-year-old female was referred to our clinic with a 3-month history of a painless mass on the anterior right shoulder. The patient had no history of trauma or constitutional symptoms. Physical examination showed a 6 × 3 cm elastic soft mass on the anteromedial aspect of the right humerus. The mass was non-tender, well circumscribed, and distinct from surrounding tissue, and did not pulsate. The overlying skin showed none of reddening, increased warmth and vein distention. Neurological examination and pulses of the upper limbs were normal. Results of laboratory tests were within normal limits.

Plain radiography of the right shoulder showed no abnormal calcifications and no abnormalities of the humerus. MRI showed that the mass was well defined and located between the deltoid and greater pectoral muscles (Fig. 1). The mass generally showed low-intensity signals on T1-W and high-intensity signals on T2-W images. There were areas that showed high-intensity signals on T1-W, and low-intensity signals on T2-W images. With fat-suppression sequences using short T1 inversion recovery (STIR), the mass showed generally high-intensity signals. After intravenous administration of a gadolinium-based contrast material, the tumor image was weakly enhanced. Thallium scintigraphy showed no intense uptake in the tumor.

Received September 10, 2010; revision accepted for publication December 16, 2010. doi: 10.1620/tjem.223.75
Correspondence: Takatoshi Ohno, M.D., Ph.D., Department of Orthopaedic Surgery, Gifu University School of Medicine, 1-1 Yanagido, Gifu 501-1194, Japan.
e-mail: takaohno@gifu-u.ac.jp

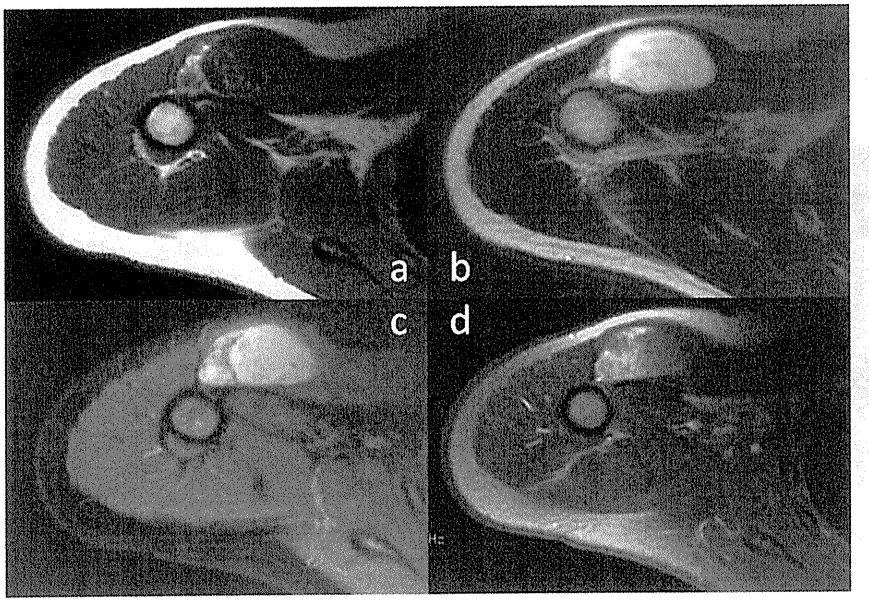

Fig. 1. MRI of the right shoulder of a 12 year-old female.
a. T1-weighted axial image showing an intra-muscular encapsulated mass. The mass is almost homogenous with low-intensity signals and contains a few high-intensity regions.
b. T2-weighted axial section image. The mass shows mostly high-intensity signals.
c. STIR axial section showing no suppression of the signal intensity of the mass, while subcutaneous fat areas are well suppressed.
d. T1-weighted Gd-DPTA-enhanced axial section showing heterogeneous enhancement of the mass.

Therefore, it was considered that alternative diagnoses include hemorrhage after rupture of muscles, myxoma, neurinoma as a benign tumor, and myxoid liposarcoma as a malignant tumor.

Due to the findings above, our clinical impression was that it was not a lipomatous tumor.

A biopsy was considered essential to make a definite diagnosis. An excisional biopsy was chosen because it could preserve the neurovascular band in case of additional resection if the tumor turned out to be malignant.

During the operation, the deltoid muscle was split and an incision was made directly into the tumor. There was no invasion found into any of the surrounding tissue, and the mass was completely excised. Macroscopically, the mass was well-circumscribed, elastic soft, yellowish and homogenous.

Histopathological examination showed the tumor to be well encapsulated. Spindle-shaped or stellate cells were embedded in the myxoid matrix, and a few small irregular clusters of mature fat cells were separated by connective tissue septa of varying thickness. There was a variable degree of cellular differentiation, and vascularization was clearly evident. There were some immature, lipoblast-like cells and mesenchmal cells dispersed throughout (Fig. 2). Ultrastructurally, the tumor cells were irregularly stellate, and cytoplasmic projections were observed engulfing the surrounding myxoid stroma, resulting in a vacuolated appearance. The cytoplasm was rich in filaments, contained small vesicles, which were focally clustered, and also contained vacuoles. A few cells possessed fat droplets (Fig. 3).

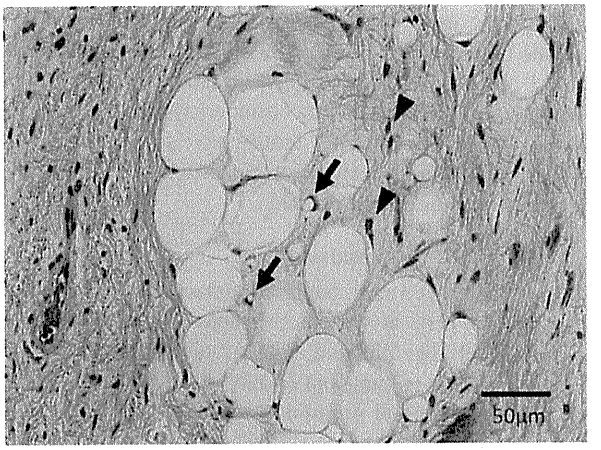

Fig. 2. The tumor section stained with Hematoxylin and eosin.
Shown are a few small irregular clusters of mature fat cells that are separated by connective tissue septa. Some lipoblast-like cells and mesenchymal cells are indicated with arrows and arrowheads, respectively. Atypical cells are not present. (× 40)

These features were consistent with lipoblastoma, and myxoid liposarcoma is considered as one of the differential diagnosis. Finally, we diagnosed the tumor as a lipoblas-

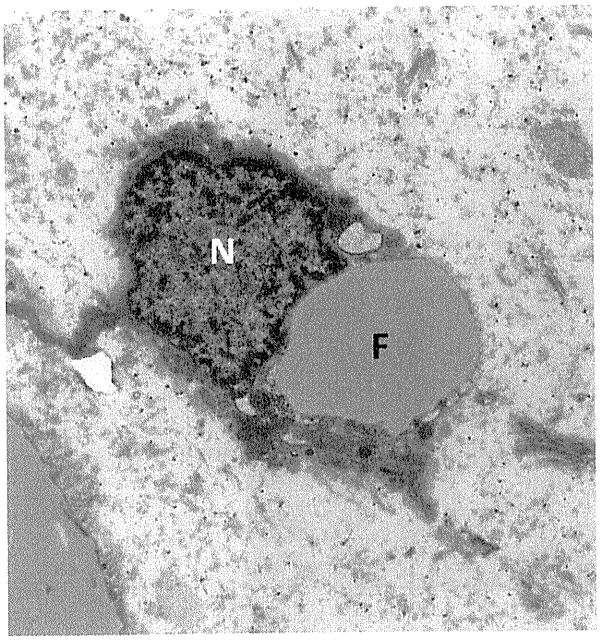

Fig. 3. Electron micrograph of the tumor.
A tumor cell presented in this picture contains fat droplet (N: nucleus, F: fat droplet).

toma for the reason that there were many mature fat cells, no atypical cells and small amount of vascularization for a myxoid liposarcoma. Furthermore, the lobulated appearance of the tumor, which is characteristic of lipoblastomas, supported this diagnosis. The postoperative course was uneventful and no recurrence was observed 5 years after the operation. The patient and her family have provided permission to publish these features of her case, and the identity of the patient has been protected.

Discussion

Lipoblastoma is a rare, benign neoplasm that consists of immature fat cells at various degrees of maturity and occurs exclusively in childhood, with a male predominance between 1.5 and 3:1 (Chung and Enzinger 1973; Stringel et al. 1982). It has a good prognosis, and does not behave aggressively or metastasize, and therefore the treatment of choice is complete but conservative excision (Chung and Enzinger 1973; Mentzel et al. 1993; Coffin 1994; Gilbert et al. 1996). This type of tumor is rare in patients older than 8 years, however, it has been reported in a number of patients over 10 years of age (Reinders et al. 1983; Jimenez 1986; Gisselsson et al. 2001). In the present report, the patient was 12 years old and was considered relatively old for the condition, and hence it was considered to be rare. (Table 1)

Pathological features of lipoblastoma include a wide spectrum of adipocytic differentiation, in which mono- and multivacuolated lipoblasts are admixed with mature adipocytes. The adipocytic cells are often set in a variably myxoid matrix containing spindle or stellate mesenchymal cells,

Table 1. A review of the age of lipoblastoma cases.

	year	cases	age (mo.)	mean (mo.)
Chung & Enzinger	1973	35	0 - 84	12
Mentzel et al.	1993	14	0 - 72	32.4
Hicks et al.	2001	25	2 - 120	20
Chun et al.	2001	7	3 - 29	15.6
Gisselsson et al.	2001	16	8 - 156	45.1
Jung SM et al.	2005	16	5 - 49	11.5
Moholkar S et al.	2006	12	6 - 72	18
Present patient	2010	1	144	—

mo., months.

and the tumor is usually organized into lobules, separated by fibrous septae (Weiss and Goldblum 2008).

The ultrastructural features of lipoblastoma are variable. As in normal developing fat, the cells show a wide morphologic spectrum ranging from immature mesenchymal cells and preadipocytes to maltivacuolar lipocytes. The lipoblasts contain numerous vesicles, round to oval mitochondria, and well-developed Golgi membranes. The present patient showed that the tumor cells contained small vesicles and vacuoles. A few cells possessed fat droplets as a mature adipocyte shows. And these cells were observed engulfing the surrounding myxoid stroma, which is compatible with the features of both lipoblastoma and mixoid liposarcoma. In fact, it is reported the principal differential diagnostic consideration of lipoblastoma is mixoid liposarcoma (Weiss and Goldblum 2008).

The origin of this disease is still unknown; however, adipocytic progenitor cells are considered to be one of the candidates of lipoblastoma. Gisselsson et al. (2001) reported chromosomal rearrangements involving band 8q12 in four lipoblastomas. Each of these alterations targeted the *PLAG1* oncogene, which encodes a zinc-finger transcription factor, expressed primarily in fetal tissues and only at very low levels postnatally. They propounded a possible mechanism of tumorigenesis of the disease is that the presence of PLAG1 overexpression transforms mesenchymal progenitor cells to lipoblastoma cells, with various degrees of proliferation and differentiation (Gisselsson et al. 2001). It might be an explanation why this disease occurs in younger age, because such progenitor cells are only present in the first few years of life (Gisselsson et al. 2001).

To achieve a diagnosis, the patient's age, gender, the location of the tumor, radiological features, and histological findings are of some help. However, diagnosis in somewhat older patients can be problematic and, to a degree, arbitrary (Mentzel et al. 1993). Mentzel et al. (1993) presented a patient diagnosed with myxoid liposarcoma that could be called a lipoblastoma if the patient had been 10 years younger. In the present report, the patient age was relatively old and it was difficult to make a differential diagnosis between myxoid liposarcoma and lipoblastoma.

Reiseter et al. (1999) reported that MRI is an essential tool for diagnosis and preoperative evaluation of lipoblastoma. MRI can show anatomical detail, which is essential for successful radical tumor excision. Also, in general, although lipoblastoma mostly gives a high-intensity signal on both T1-W and T2-W images, it may be hypointense and more heterogeneous with subcutaneous fat on the T1-W image (Letourneau et al. 1993; Gilbert et al. 1996). However, in the present patient, the mass was found to be generally homogenous with low-intensity signals on T1-W, and with high-intensity signals on T2-W images. Furthermore, with fat-suppression sequences, the mass showed generally high-intensity signals. These findings are non-specific, but they are not consistent with lipomatous tumors. In this patient, it is possible that the tumor contained a mucinous matrix, resulting in generally low-intensity signals on the T1-W image. Thus, it should be noted that lipoblastoma could show atypical MRI findings.

Conclusion

We present a patient with lipoblastoma that shows unusual MRI findings.

References

Chung, E.B. & Enzinger, F.M. (1973) Benign lipoblastomatosis. An analysis of 35 cases. *Cancer*, **32**, 482-492.

Chun, Y.S., Kim, W.K., Park, K.W., Lee, S.C. & Jung S.E. (2001) Lipoblastoma. *J. Pediatr. Surg.*, **36**, 905-907.

Coffin, C.M. (1994) Lipoblastoma: an embryonal tumor of soft tissue related to organogenesis. *Semin. Diagn. Pathol.*, **11**, 98-103.

Hicks, J., Dilley, A., Patel, D., Barrish, J., Zhu, S.H. & Brandt, M. (2001) Lipoblastoma and lipoblastomatosis in infancy and childhood: histopathologic, ultrastructural, and cytogenetic features. *Ultrastruct. Pathol.*, **25**, 321-333.

Gilbert, T.J., Goswitz, J.J., Teynor, J.T. & Griffiths, H.J. (1996) Lipoblastoma of the foot. *Skeletal Radiol.*, **25**, 283-286.

Gisselsson, D., Hibbard, M.K., Dal Cin, P., Sciot, R., His, B.L., Kozakewich, H.P. & Fletcher, J.A. (2001) PLAG1 alterations in lipoblastoma: involvement in varied mesenchymal cell types and evidence for alternative oncogenic mechanisms. *Am. J. Pathol.*, **159**, 955-962.

Jimenez, J.F. (1986) Lipoblastoma in infancy and childhood. *J. Surg. Oncol.*, **32**, 238-244.

Jung, S.M., Chang, P.Y., Luo, C.C., Huang, C.S., Lai, J.Y. & Hsueh, C. (2005) Lipoblastoma/ lipoblastomatosis: a clinicopathologic study of 16 cases in Taiwan. *Pediatr. Surg. Int.*, **21**, 809-812.

Letourneau, L., Dufour, M. & Deschenes, J. (1993) Shoulder lipoblastoma: magnetic resonance imaging characteristics. *Can. Assoc. Radiol. J.*, **44**, 211-214.

Mentzel, T., Calonje, E. & Fletcher, C.D. (1993) Lipoblastoma and lipoblastomatosis: a clinicopathological study of 14 cases. *Histopathology*, **23**, 527-533.

Moholkar, S., Sebire, N.J. & Roebuck, D.J. (2006) Radiological-pathological correlation in lipoblastoma and lipoblastomatosis. *Pediatr. Radiol.*, **36**, 851-856.

Reinders, J., Noyez, L., Munting, J. & van den Tweel, J. (1983) A benign inguinal lipoblastoma in a 14-year-old girl. A case report. *Acta Chir. Belg.*, **83**, 427-429.

Reiseter, T., Nordshus, T., Borthne, A., Roald, B., Naess, P. & Schistad, O. (1999) Lipoblastoma: MRI appearances of a rare paediatric soft tissue tumour. *Pediatr. Radiol.*, **29**, 542-545.

Stringel, G., Shandling, B., Mancer, K. & Ein, S.H. (1982) Lipoblastoma in infants and children. *J. Pediatr. Surg.*, **17**, 277-280.

Weiss, S.W. & Goldblum, J.R. (2008) *Enzinger and Weiss's SOFT TISSUE TUMORS*, 5th ed., Mosby, Philadelphia, PA, pp. 452-456.

右前腕腫瘍の１例

岐阜大学医学部　整形外科　　大島康司、大野貴敏、清水克時
同　　看護学科　　西本　裕
岐阜大学病院　　病理部　　浅野奈美、広瀬善信

【症　例】21歳、男性。
【主　訴】右前腕遠位部腫瘤。
【既往歴】アトピー性皮膚炎。
【家族歴】特記事項なし。
【現病歴】2002年頃から右前腕部に違和感が生じていたが放置。2007年10月頃より右前腕遠位部の腫瘤を自覚。その後近医を受診し、2008年8月当科を紹介され受診した。
【入院時現症】右前腕部遠位部掌側に径約3×4cmの弾性硬の腫瘤を触知した。皮膚との癒着なし。腫瘍床との可動性は不良。境界は比較的明瞭。発赤、熱感、圧痛なし。右前腕の回内が45°と可動域制限を認めた。
【血液検査所見】LDH 247(125-225 IU/L) 尿酸 7.6(2.5-6.9mg/dl) CRP 0.27(0.20mg/dl以下)と若干の上昇を認めたが他に異常なし。
【画像所見】単純X線：右橈骨遠位骨幹端から骨幹部にかけて辺縁骨硬化を伴う地図状の骨透亮像を認める。骨膜反応は明らかでない(図1)。
CT：同部位に長径約4cm大の溶骨性病変を認め、掌側の皮質は消失し骨外腫瘤も認める(図2・3)。
MRI：腫瘍はT1強調像で筋肉とiso intensityを示す。T2強調像では概ね高信号を示すが、骨外腫瘍は不均一な信号低下の見られる部位も存在する。Gd造影では、骨内の腫瘍が比較的均一に造影効果を認めるのに対し、骨外腫瘍は不正な造影不良域を認める。骨外腫瘍の境界はやや不明瞭ではあるが、軟部組織への明らかな浸潤傾向は認めない(図4・5・6)。
骨シンチ：右前腕腫瘍に一致して中程度の異常集積を認めるが、他の部位への異常集積は認めない(図7)。
【治療経過】画像所見等から経過の長い良性病変が疑われたが、皮質の消失と骨外腫瘤の存在から悪性腫瘍も否定できず、切開生検を施行した。その結果、線維性の良性腫瘍が疑われたが、低悪性度の悪性腫瘍も完全に否定できなかった。後日、腫瘍辺縁切除術を施行した(図8・9・10)。腫瘍は被膜に被われ、方形回内筋との癒着は認めなかった。骨内の腫瘍切除の際、一部腫瘍内切除となった。掻爬後の骨内を高速ダイアモンドバーにて十分掘削し、液体窒素スプレーによる凍結処理を行った。次いで骨折予防のため、プレートを設置した。
【病理所見】紡錘形細胞の増殖がみられ、背景には線維性と思われる基質が比較的豊富に見られる。核異型や分裂像は目立たない。骨・軟骨組織も少数見られるが異型は乏しい(図11)。
免疫染色では、SMAが一部で陽性を示したが、S100, デスミン, CD34, CD31, Cytokeratin, EMAは陰性であった。MIB-1陽性率は極低値であった。以上よりDesmoplastic fibromaと診断した。
【考察・討論】検討会では病理診断に異論はなかった。腫瘍の発生部位に関しての議論では、腫瘍が偏心性に存在し、骨髄内に硬化性変化を認めることより、骨膜/骨皮質より発生したとの意見があった。また軟部に発生したデスモイドが骨内に浸潤したとの意見もあった。Desmoplastic fibroma of boneは原発性骨腫瘍のうち0.1%-0.3%と非常に稀であり、10歳代に多いが幅広い年齢層にわたって発生する。画像上、地図状の骨溶解像を認めるが、本例のように厚い辺縁硬化像を呈することは少ない。掻爬術では再発率が高いため広範切除に準じた治療が必要とされる。また骨肉腫への悪性転化の報告があり[1]、本例においても注意深い経過観察が必要と考える。
【参考文献】

1) Abdelwahab I. F et al: Osteosarcoma arising in a Desmoplastic fibroma of the proximal tibia. Am J Roentgenol. 178(3): 613-615, 2002.

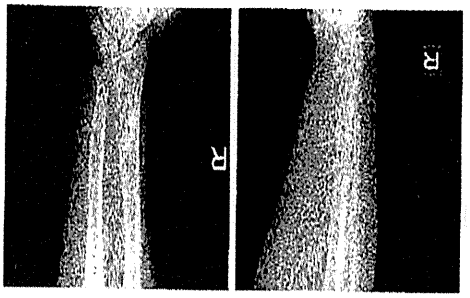

図1　単純レントゲン

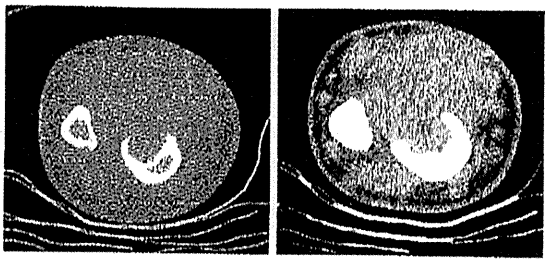

骨条件　　軟部条件

図2　CT

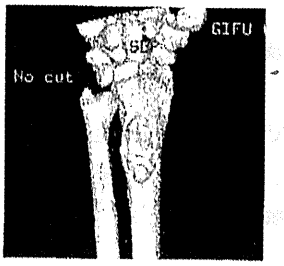

図3　3-D CT

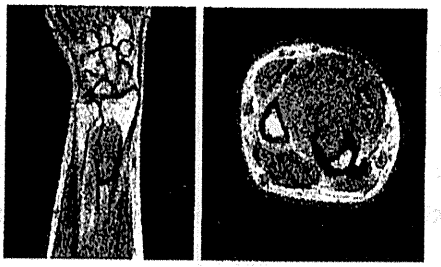

図4　MRI(T1W)

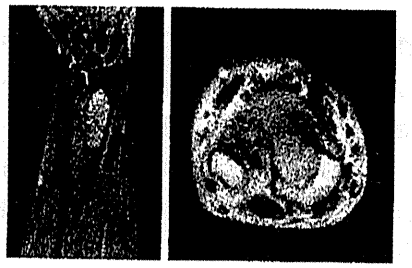

図5　MRI(T2 Fat sat)

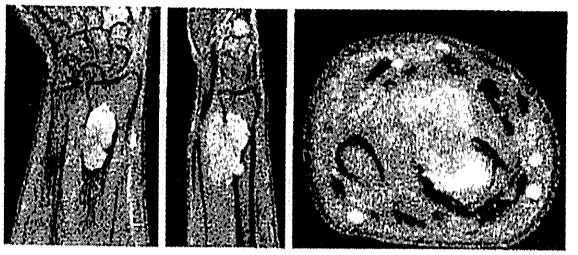

図6　MRI(T1W, Gd造影)

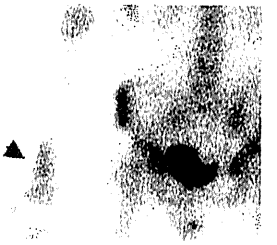

図7　骨シンチグラム

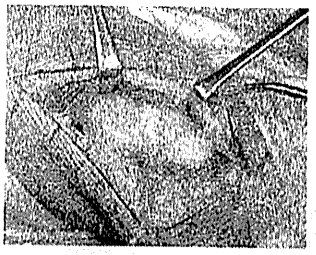

図8　術中写真

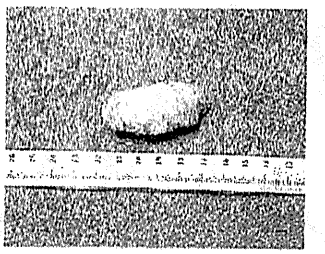

図9　摘出標本

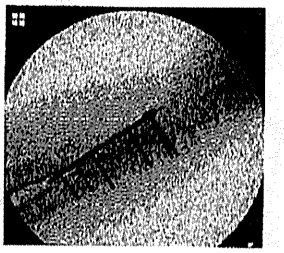

図10　術後単純レントゲン

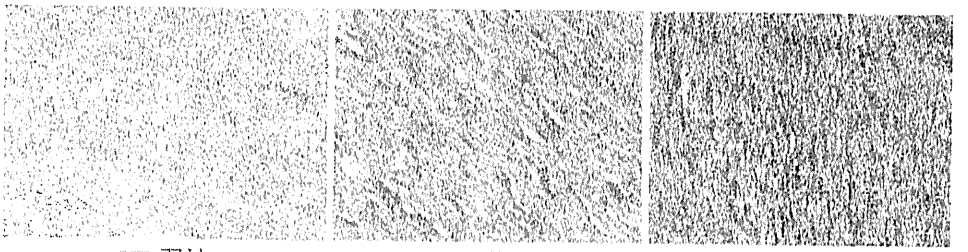

HE 弱拡　　HE 強拡　　Massontrichrom 染色

図11　病理組織像

臨床室

緩和治療においてMohsペーストが有用であった悪性軟部腫瘍の1例*

濱田哲矢　平岡弘二　庄田孝則　福島信広　永田見生**

[整形外科 62巻10号：1097～1099，2011]

高齢者や終末期の医療において，根治的治療ができない悪性軟部腫瘍例を経験することがあるが，このような患者では生活の質（QOL）や介護者の負担が問題となる．今回われわれは，Mohsペーストを使用し局所コントロールを行うことで緩和治療に有用であった悪性軟部腫瘍例を経験したので報告する．

症　例．95歳，女．

主　訴：右殿部腫瘤．

家族歴・既往歴：特記すべきことはない．

現病歴：1994年2月ごろ，右大腿部近位外側に腫瘤が出現し，徐々にサイズが増大するために当科を初診した．

初診時所見：右大腿骨大転子部皮下に直径7 cmの腫瘤を認めた（図1）．

生検術を施行し，悪性軟部腫瘍であったため広範囲切除術予定とした．しかし高齢であり本人・家族が侵襲の大きい手術を拒否したため辺縁切除術を施行した．

病理組織学的所見：悪性線維性組織球腫であった．

術後経過：術後4ヵ月で再発したため本人・家族を説得し追加切除術＋植皮を施行したが，術後2年11ヵ月で再々発した．腫瘍学的，年齢的に再手術困難と判断し，また本人・家族の手術拒否もあったため放射線治療（30 Gy）を施行し，自宅で緩和治療を行うこととなった．しかしその後も腫瘍が増大し，自潰・出血を繰り返

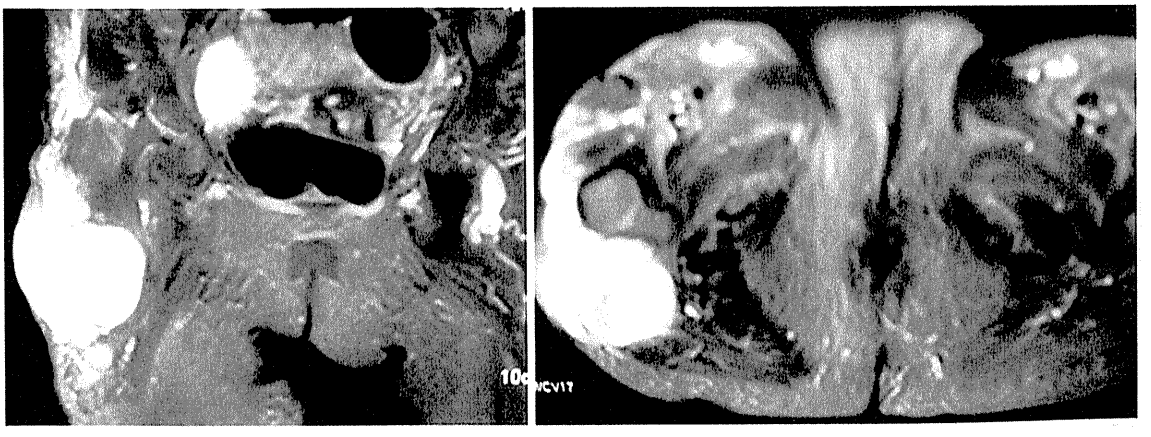

a．冠状断像　　b．軸射像

図1．初診時右股関節部MRI T2強調画像

Key words：Mohs chemosurgery, soft tissue sarcoma, terminal care

* Mohs chemosurgery for unresectable local lesion of soft tissue sarcoma；report of a case
要旨は第42回日本整形外科学会骨・軟部腫瘍学術集会において発表した．

** T. Hamada, K. Hiraoka(講師), T. Shouda, N. Fukushima, K. Nagata(教授)：久留米大学整形外科（Dept. of Orthop. Surg., Kurume University School of Medicine, Kurume）．